ELSEVIER ELSEVIER

Contents lists available at ScienceDirect

Journal of Catalysis

journal homepage: www.elsevier.com/locate/jcat



Density functional theory study of furfural electrochemical oxidation on the Pt (1 1 1) surface



Li Gong ^{a,b,d}, Naveen Agrawal ^b, Alex Roman ^c, Adam Holewinski ^c, Michael J. Janik ^{b,*}

- ^a Department of Chemistry, University of Science and Technology of China, Hefei, China
- ^b Department of Chemical Engineering, The Pennsylvania State University, University Park, PA 16802, USA
- ^c Department of Chemical and Biological Engineering, University of Colorado, Boulder, CO 80309, USA
- ^d College of Environment, Zhejiang University of Technology, Hangzhou 310014, China

ARTICLE INFO

Article history: Received 28 January 2019 Revised 9 April 2019 Accepted 9 April 2019 Available online 23 April 2019

Keywords: Electrocatalysis DFT Biomass Electrooxidation

ABSTRACT

Electro-oxidation of furfural may allow for tunability of product selectivity by varying the electrode potential. We have applied density functional theory (DFT) to investigate the electrocatalytic oxidation mechanism on the Pt (1 1 1) surface. The potential-dependent reaction free energy profiles for furfural electrocatalytic oxidation to furoic acid, succinic acid, maleic acid, and maleic anhydride are reported. After comparing several possible furfural oxidation paths, we conclude that the electro-oxidation of furfural preferentially proceeds to furoic acid, with further oxidation slowed by difficult C—C bond dissociation. Oxidation beyond furoic acid can proceed to succinic acid via 2(3H)-furanone as an intermediate and to maleic acid and maleic anhydride via 2(5H)-furanone as an intermediate. The rate of these processes is likely limited by the decarboxylation of furoic acid. DFT analysis of elementary step thermodynamics and kinetics suggests that the selectivity between furoic acid, succinic acid, maleic acid, or other oxidized products is tunable by varying the electrode potential. Initial experimental results show furoic acid as the most significant product (>80% selectivity) at 0.9 V-RHE on a Pt electrode, in agreement with DFT results. These results broaden our fundamental understanding into electrocatalytic oxidation of furfural, which is applicable in upgrading renewable biomass derivatives.

© 2019 Elsevier Inc. All rights reserved.

1. Introduction

Upgrading of renewable biomass derivatives to commercially relevant compounds can help to meet growing energy demands and increase infrastructure sustainability [1,2]. Furfural is a promising biomass-derived synthetic platform species with numerous chemical outlets [3]. Through partial oxidation of furfural, products with increasing molar ratio of O to C atoms (furanones, acid anhydrides and dicarboxylic acids) are accessible [4] and these species find wide downstream use in applications as diverse as polyester resins, surface coatings, solvents, plastics, food additives, and pharmaceuticals [5].

Furfural oxidation could provide an alternative to fossil feedstock production of furanones, furoic acid, maleic anhydride (MAN), maleic acid (MA) and succinic acid (SA) [6], but scalable production routes remain elusive due to poor selectivity and energy efficiency. Driving reactions with electric potential, such as the electro-oxidation of furfural, could be a promising green

* Corresponding author. E-mail address: mjanik@psu.edu (M.J. Janik). method using electricity derived from solar, wind and geothermal sources. Electro-oxidation may also allow improvements in the selectivity of furfural oxidation. Most previous studies of furfural partial oxidation to acid anhydrides and dicarboxylic acids utilized either oxygen or hydrogen peroxide as the oxidant together with heterogeneous catalysts. These reactions may involve the use of expensive oxidants, elevated temperatures (50-320 °C), low yields and low selectivity to target products, or deactivation of the catalysts [7–11]. Electro-oxidation may offer different reaction paths and selectivity control not offered in chemical oxidation, motivating our mechanistic analysis. Several groups have proposed possible furfural reduction mechanisms on the basis of detected intermediates [11,12], but less is known of the furfural electrooxidation mechanism. Electrocatalytic oxidation has been studied for biomass-derived species conversion including conversion of 5-hydroxymethylfurfural and glycerol [13-17].

Electrical potential could be used to alter the energy landscape of a reaction network. As the potential shifts by $E-E^0$, reaction energies of intermediates also shift by $nF(E-E^0)$, where n is the number of electrons transferred to form the product and F is Faraday's constant (which is unnecessary if electron-Volts are used as the energy unit). Favorability to form different oxidation products will vary

with electrode potential, with larger n values corresponding to larger sensitivity to potential. Therefore, reaction selectivity can in principle be controlled by the applied potential. Electrocatalytic furfural oxidation could offer other advantages [17], such as: (1) low operating temperatures and pressures; (2) electric potential could be easily controlled uniformly across a reactor, compared with an O_2 pressure that varies with conversion throughout a reactor; and (3) H_2O can serve as the O-source instead of higher-cost O_2 gas or other oxidant.

The electrocatalytic oxidation of furfural is at its initial stage, and a mechanistic understanding of the catalytic reactions can guide catalyst design for a selective process. Among the various metal nanoparticles, platinum catalyzes electrocatalytic oxidation reactions including the methanol oxidation reaction (MOR), the ethanol oxidation reaction (EOR) as well as the dimethyl ether oxidation, and shows high stability [18-20]. Pt-based catalysts have also been employed in biomass electro-oxidation [21,22]. Herein, density functional theory (DFT) methods are used to explore the furfural electrochemical oxidation reaction over the Pt (1 1 1) surface. We propose possible furfural oxidation paths and key intermediates. The possible initial steps of furfural oxidation are given greater attention as dictating selectivity, by considering elementary step kinetics and thermodynamics. These results will help guide catalyst design for furfural electro-oxidation. Initial experimental electro-oxidation results are also presented, showing furoic acid as a major product at 0.9 V-RHE.

2. Methods

DFT calculations were performed within the Vienna Ab initio simulation package (VASP, version 5.3.5), using the periodic supercell approach. The projector augmented wave (PAW) method was used for electron-ion interactions [23,24]. The Perdew-Burke-Ernzerhof functional [25] with dispersion correction (PBE-D3) [26] described the electron-electron exchange and correlation energies [27,28]. PBE-D3 was previously used to examine furfural catalysis and provided mechanistic behavior consistent with experiment [29]. A plane wave basis set is used with an energy cutoff of 450 eV. For geometry optimization, the convergence criteria of the forces acting on atoms was 0.05 eV Å⁻¹, while the energy threshold-defining self-consistency of the electron density was 10^{-5} eV. Transition state structure searches used the climbing image nudged elastic band (CI - NEB) method. Atomic forces at the transition state met the same 0.05 eV force Å⁻¹ convergence and a single imaginary vibration mode along the reaction coordinate was confirmed [30].

2.1. Model

For gas phase species, a cubic cell of $15 \times 15 \times 15$ Å was used. The Pt (1 1 1) metal slab was constructed with a 3×3 unit cell composed of five atomic layers. The bottom three layers were frozen at their bulk lattice positions. The vacuum region between the slabs, before adding adsorbates, was 20 Å to avoid interactions between periodic slabs. In this initial mechanistic analysis, we do not consider solvation of surface adsorbed species or the charging of the electrode/electrolyte interface. Spurious slab-to-slab dipole interactions were corrected (VASP keywords LDIPOL = TRUE, IDIPOL = 3).

2.2. Elementary electrochemical reaction energies

The geometries of all surface furfural oxidation intermediates were fully optimized, considering multiple initial adsorption configurations to determine the lowest energy structures. All relative

energies presented herein are zero point vibrational energy (ZPVE) corrected and include a vibrational entropy term. The free energy of an adsorbed intermediate is calculated as:

$$G_{intermediates} * = E_{intermediates} * + E_{ZPVE} + E_{vib} - TS_{vib}$$
 (1)

where $E_{intermediate}^*$ is the DFT optimized energy of the adsorbed intermediate, E_{ZPVE} is the zero-point vibrational energy, E_{vib} is the internal energy stored in vibration at 300 K, and TS_{vib} represents the vibrational entropy of the adsorbed species at 300 K. E_{vib} can be calculated using the Boltzmann population of vibrational states as stated in Eq. (2), where v_i is vibrational frequency of normal mode i calculated through the harmonic approximation, h is Planck's constant and k is Boltzmann's constant.

$$E_{vib} = \sum_{i} \frac{hv_i}{\left(exp\left(\frac{hv_i}{kT}\right) - 1\right)}$$
 (2)

The optimized energy of each surface intermediate $C_X H_Y O_Z^*$ is calculated relative to adsorbed furfural using the computational hydrogen electrode (CHE) approach [31]. Relative energies represent the reaction energy to form any adsorbed intermediate from adsorbed furfural via the reaction:

furfural
$$(C_5H_4O_2)^* \to C_XH_YO_Z^* + (2X - Z - 8)H_2O_{(l)}$$

 $+ (5 - X)CO_{2(gas)}$
 $+ (20 + 2Z - 4X - Y)(H^+ + e^-)$ (3)

Relative energies at a potential (U) on the CHE (or, equivalently, relative hydrogen electrode, RHE) scale are calculated:

$$\begin{aligned} RE(U) &= G_{C_X H_Y O_Z^*} - G_{furfural^*} + \left(\frac{20 + 2Z - 4X - Y}{2}\right) G_{H_2} \\ &+ (2X - Z - 8)G_{H_2 O(I)} + (5 - X)G_{CO_2(g)} \\ &- (20 + 2Z - 4X - Y)eU \end{aligned} \tag{4}$$

 $G_{C_XH_YO_Z^*}$ is the ZPVE corrected free energy of the adsorbed intermediate, $G_{furfural^*}$ is the free energy of furfural on the surface, and G_{CO_Z} , G_{H_Z} and G_{H_ZO} are the free energies of gas phase CO_Z , H_Z and H_ZO , respectively. The value of e in the final term is the absolute value of the electron charge. The free energies of isolated CO_Z , H_Z and H_ZO were obtained from calculations of a single molecule in a cubic unit cell of side length 15 Å. Statistical mechanics corrections for the gas phase molecule ($E_{vib} + E_{trans} + E_{rot} - TS_{total}$) (provided in Table S1) and PV corrections assuming ideal gas behavior were included to determine the free energy of H_ZO_Z (g) and CO_ZO_Z (g) at 1 atm and the free energy of CO_ZO_Z (g) at 1 atm and the free energy of CO_ZO_Z (g) at 0.03 atm—the vapor pressure of water at room temperature [32]. Where CO_ZO_Z includes translational and rotational entropy terms along with vibrational entropy for the gas phase molecules.

2.3. Adsorption energies

The adsorption energies of surface species were calculated using Eq. (5)

$$\Delta E_{ads} = E_{species+surface} - E_{species} - E_{surface}$$
 (5)

where $E_{species}$ is the energy of the isolated intermediate, $E_{surface}$ is the energy of the bare surface, and $E_{species+surface}$ is the energy of the intermediate adsorbed on the surface. A negative ΔE_{ads} corresponds to a stable adsorbate–surface system.

2.4. Potential-dependent activation barriers

Activation barriers as a function of electrode potential U were calculated based on the Butler-Volmer formalism as done previously in our group [33,34]:

$$E_{act}(U) = E_{act}^{0}(U^{0}) - \beta e\left(U - U^{0}\right) \tag{6}$$

For reaction: $(AH)^* \rightarrow A^* + H^*$

$$U^{0} = \frac{G_{A^{*}} + \frac{1}{2}G_{H_{2}^{*}} - G_{(A^{*} + H^{*})}}{e}$$
 (7)

For reaction: $A^* + OH^* \rightarrow (A-OH)^*$

$$U^{0} = \frac{G_{(A^{*}+0H^{*})} + \frac{1}{2}G_{H_{2}^{*}} - G_{A^{*}} - G_{H_{2}0}}{e}$$
 (8)

For reaction: $A^* + O^* \rightarrow (A-O)^*$

$$U^{0} = \frac{G_{(A^{*}+0^{*})} + G_{H_{2}^{*}} - G_{A^{*}} - G_{H_{2}0}}{2e}$$
 (9)

where E_{act}^0 is the activation barrier obtained from DFT calculation; U^0 is the equilibrium potential obtained from (7-9) for removing/ adding the H/OH/O species to the unit cell; β is a reaction symmetry factor denoting the relationship between the activation barrier and reaction energy change [35]. β is typically between 0.3 and 0.7 and we approximate that β is equal to 0.5 for all one electron steps. For O^* addition steps, we presume β is equal to 1.5, approximating that the initial oxidation of water to form OH* is equilibrated and the second electron transfer occurs during O addition. This method allows us to approximate potential dependent activation barriers by calculating the transition state for the non-electrochemical X-H dissociation or C-OH formation step, then assign the calculated barrier to the potential at which the H/OH/O species in the unit cell has the same chemical potential of the water, protons, and electrons involved in generating it. The barrier is taken to have reached 0 when Eq. (5) produces a negative barrier.

2.5. Experimental methods

Electrochemical oxidation of 100 mM furfural (Sigma Aldrich, distilled before use) in 0.25 M perchloric acid electrolyte (Millipore Sigma Suprapure) was carried out in a differential packed-bed electrochemical reactor (ID 3 mm). 40% Pt/C (Premetek) was used as a working electrode; a packed bed was formed by depositing the powder on porous carbon cloth, which spanned the reactor perpendicular to the flow. Electrolyte was deaerated with Ar for at least 20 min, then flowed at 0.05 mL/min. 2 mg Pt basis was used for each trial, with ECSA determined by underpotential-deposited hydrogen stripping. Steady state was established with a potentiostatic hold for 30 min, followed by sample collection for another 30 min. An RHE reference electrode and Pt counter electrode (both flame polished) were located in bridge tubes that met the flow channel by tapped ports at the sides. Another port permitted gas phase analysis by differential electrochemical mass spectrometry (DEMS). The solution phase products observed at the outlet were characterized using LC/MS-APCI/ESI (Atmospheric Pressure Chemical Ionization and Electron Spray Ionization). UV-DAD (Diode Array Detector) measurements were used to quantify the identified products, furoic acid (251 nm), 5-hydroxyfuranone (UV = 200 nm), maleic acid (UV = 215 nm). 5-Hydroxyfuroic acid was quantified via H-NMR using an internal standard. After confirming no other products except CO2 could be detected by LCMS, DEMS, or NMR, CO₂ was assigned to the remaining electron balance.

3. Results and discussion

In Section 3.1, we propose possible furfural electro-oxidation paths based on previous studies of furfural oxidation. In Section 3.2, we report the optimal structures of the intermediates on the Pt (1 1 1) surface. In Section 3.3, we use the computed energies of the intermediates to calculate the thermodynamics of furfural oxi-

dation to various products over the Pt $(1\ 1\ 1)$ surface. In Section 3.4, we compare the initial steps of each path for furfural oxidation, including activation barriers. In Section 3.5, we construct the reaction energy diagrams for the overall reaction paths for furfural oxidation on the Pt $(1\ 1\ 1)$ surface.

3.1. Proposed furfural oxidation mechanisms

Based on the previous experimental studies of furfural oxidation by Yin et al. [36,37], Zhang et al. [9] and Granados et al. [11], four different reaction paths for furfural electro-oxidation are proposed and considered, summarized in Schemes 1-4. In these schemes, (H⁺ + e⁻) or CO₂ generated and H₂O molecules converted are left off for clarity. In these paths, we assume maleic acid and maleic anhydride do not convert to succinic acid, as it has been reported that maleic acid and maleic anhydride are stable products at mild conditions [38]. We note that some species are labeled as radicals in Schemes 1-4 to provide clarity as to the chemical composition of the intermediate, though binding of the unsaturated atom to the surface would occur and the unpaired electron would be involved in a filled bonding state. We also have chosen a limited set of paths for consideration based on previous work, much of which is based on observation of partial oxidation intermediates in the fluid phase rather than a direct consideration of surface species.

In Path 1, furfural initially oxidizes to furoic acid, which then decarboxylates to a furyl intermediate. The furfural is first oxidized by dissociating the C-H bond of the aldehyde group to form F-CO (F denotes a furanic ring), followed by furoic acid formation. Furoic acid is oxidized to 2-hydroxyfuran. 2-hydroxyfuran is in equilibrium with epoxidised-furan, 2(3H)-furanone and 2(5H)-furanone [39]. These species branch to Paths 1-A, B, C. Epoxidized -furan could be oxidized to maleic acid (1-A); 2(3H)-furanone could be oxidized to succinic acid (1-B), whereas 2(5H)-furanone could be oxidized to maleic acid and maleic anhydride (1-C) [11,38]. The presence of the three tautomeric species that branch to Paths 1-A. B. and C influences the selectivity of furfural oxidation [39]. Though Path 1 initiates with furoic acid formation followed by decarboxylation, decarbonylation may occur by removing CO before C-OH bond formation [40,41]. Besides, decarboxylation could also occur by removing CO2 from a furoic acid molecule. We determined all the energetics for both CO and CO2 removal through Path 1.

In Path 2, furfural is initially oxidized by breaking a C—H bond of the furan ring and forming the furfuryl intermediate ($C_5H_3O_2^*$), as shown in Scheme 2. The furfuryl intermediate is further oxidized to maleic anhydride. Lan et al. has reported furfural oxidation to maleic anhydride on a $H_5PV_2Mo_{10}O_{40}$ catalyst through this path [12]. Alternatively, the furfuryl intermediate could also attack the C=O bond of another furfural and initialize polymerization [12]. Though we do not consider polymerization explicitly, it is important to examine both kinetics and thermodynamics of furfuryl intermediate formation. Significantly greater stability of the adsorbed furfuryl intermediate, in comparison to its gas phase radical counterpart, should result into slower polymerization at the surface. We therefore hypothesize that surface polymerization can be neglected in our initial examination of furfural electro-oxidation.

In Path 3, furfural is initially oxidized by addition of an O atom to a double bond of the furanic ring. The less sterically hindered C=C bond is epoxidized, as proposed by Granados et al. [11]. The epoxidized furfural rapidly undergoes a rearrangement and further oxidation to maleic acid, shown in Scheme 3.

In Path 4, furfural is initially oxidized to 2-hydroxyfuran with a Baeyer-Villiger reaction of the aldehyde group of furfural. The 2-hydroxyfuran could be eventually oxidized to maleic acid,

Scheme1. Path 1: reaction mechanism through furoic acid and decarboxylation.

Scheme 2. Path 2: reaction mechanism through the furfuryl intermediate.

succinic acid and maleic anhydride through the same 1-A, 1-B, 1-C paths.

Despite the significant number of species involved in these schemes, this current study does not consider all plausible paths as we limited our analysis to these paths previously identified in the literature. As discussed below, these paths do include some steps which may not be considered elementary. We examined the reaction energies of conversions among surface species, though some reaction steps could involve desorption of an intermediate, solution phase transformation, and re-adsorption. At mildly oxidizing potentials (U < 0.4 V-RHE), the Pt surface may still have significant coverage of adsorbed H^* , and mixed oxidation/reduction paths are also plausible.

3.2. Adsorption of intermediates

The Pt (111) surface has four high symmetry surface exposed sites for adsorption: top (t), bridge (b), 3-fold hollow site (fcc and hcp). Our general approach to determining optimal adsorption configurations was to position unsaturated moieties over these high symmetry sites, with specific structures considered when preferred adsorption geometries were previously reported. Calculated adsorption energies of the key intermediates are listed in Table S2 with the corresponding adsorption configurations illustrated in Figs. S1 and S2.

On the Pt (1 1 1) surface, furfural prefers to adsorb with the furanic ring parallel with the surface and the center of the ring

Scheme 3. Path 3: reaction mechanism via epoxidation of furan ring and subsequent release of formic acid.

Scheme 4. Path 4: reaction mechanism starting with a Baeyer-Villiger oxidation of aldehyde group of furfural.

above a fcc site. The binding energy (-2.09 eV) of furfural mainly arises from interaction of the unsaturated furanic ring with the Pt (1 1 1) surface, which is consistent with the furfural adsorption geometries determined by Liu et al. [42]. Furoic acid adsorption behavior is similar to furfural. Furoic acid also preferentially adsorbs at the three-fold fcc site with the furanic ring parallel to the surface. In the most stable furanone adsorption configurations, both 2(3H)-furanone and 2(5H)-furanone interact with the Pt (1 1 1) surface through their unsaturated C=C bond. This is consistent with 2(5H)-furanone adsorption on the Pt (111) surface reported by Medlin and co-workers [43]. The most preferred structure of maleic anhydride on Pt (1 1 1), with an adsorption energy of −1.84 eV, has the olefinic group (C=C) in the ring of maleic anhydride bridged on two Pt atoms, as shown in Fig. S1. Previous DFT calculations have also found this di- σ -adsorption to be the most stable [44,45]. For maleic acid, the most stable adsorption configuration has the C=C group on the bridge site with Pt-C distances of 2.12 and 2.11 Å. For succinic acid, the molecule is adsorbed through the O atom of the carboxyl group with the Pt-O distance of 2.23 Å. Calculated adsorption energies for maleic acid and succinic acid are -2.05 and -0.96 eV, respectively.

3.3. Overall thermodynamics of furfural oxidation over the Pt (1 1 1) surface

The relative free energies of the 13 key intermediates that may occur in furfural oxidation were calculated both adsorbed to surface and in the gas phase as a function of potential. Comparing the free energies of gas phase and adsorbed species helps us to identify which intermediates are most stabilized by the Pt (1 1 1)

surface. Fig. 1 show the electrode-potential dependent relative free energies, calculated via Eq. (3), of intermediates for the surface adsorbed and gas phase species. Gas phase relative free energies do not include entropic terms other than harmonic vibrations. This allows for comparison to surface species to identify which species are best stabilized by the surface. Fig. 2 show the equilibrium potential for formation of the various intermediates on the surface or in the gas phase. Fig. S1 and S2 shows all the structures of intermediates. Tables S3 and S4 give the equilibrium formation potentials.

Equilibrium potentials for species adsorbed on the Pt (1 1 1) surface are generally lower than gas phase potentials, as most intermediates bind more strongly to the surface than furfural. Furan* (*denotes an adsorbed species) has the lowest equilibrium potential and is favorable to form from furfural at any potential relevant for electro-oxidation. Furan binds much stronger to the surface than furfural, leading to its low surface oxidation potential relative to a gas phase equilibrium potential of 0.99 V-RHE. Furan may also be formed through a non-electrochemical decarbonylation route (furfural converted to CO and furan) that would involve no net oxidation or reduction. The equilibrium potential reported corresponds only to the decarboxylation route (producing CO₂ rather than CO). At potentials less than 0.10 V-RHE, only maleic anhydride*, 2(3H)-furanone* and furoic acid* are favorable to form. With increasing potential, from 0.10 to 0.2 V-RHE, maleic acid*, β-formylacrylic acid*, maleic dialdehyde*, succinic acid*, 2hydroxyfuran* and 2(5H)-furanone* become favorable. Succinic acid is the most stable oxidation product in the gas phase, however, weaker binding makes its equilibrium potential (0.16 V, Table S2) higher than many other products as a surface species. Furoic acid

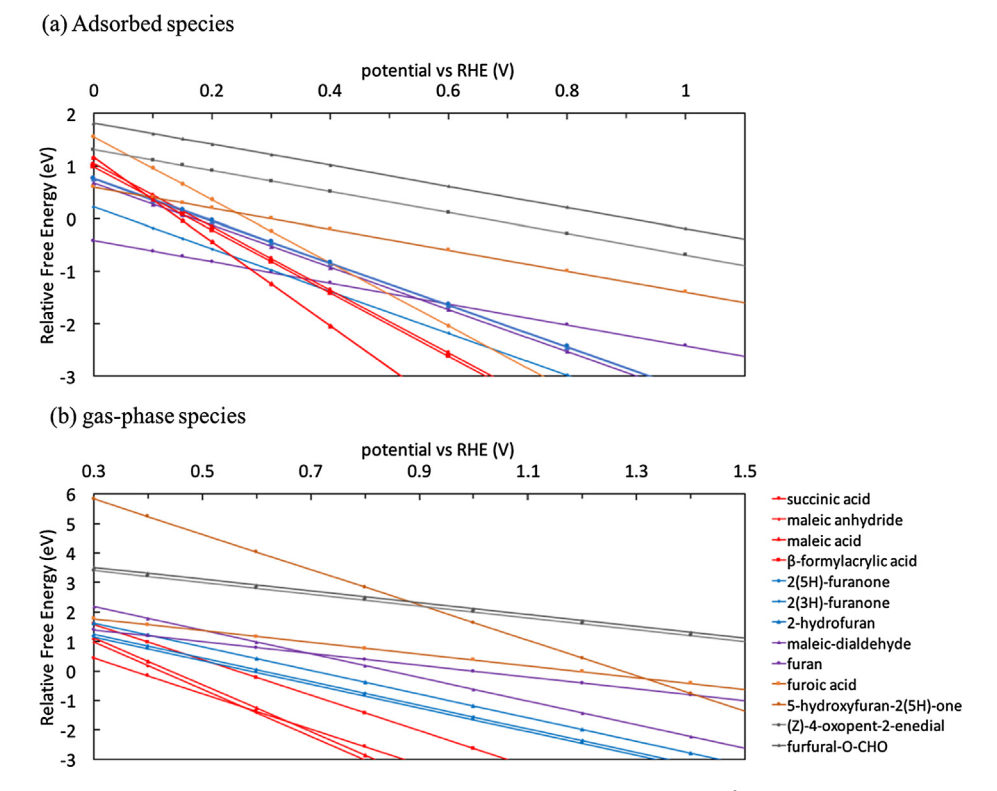


Fig. 1. Potential dependent free energies of key intermediates in furfural oxidation relative to adsorbed furfural (a) and gas phase furfural (b) calculated from Eq. (3).

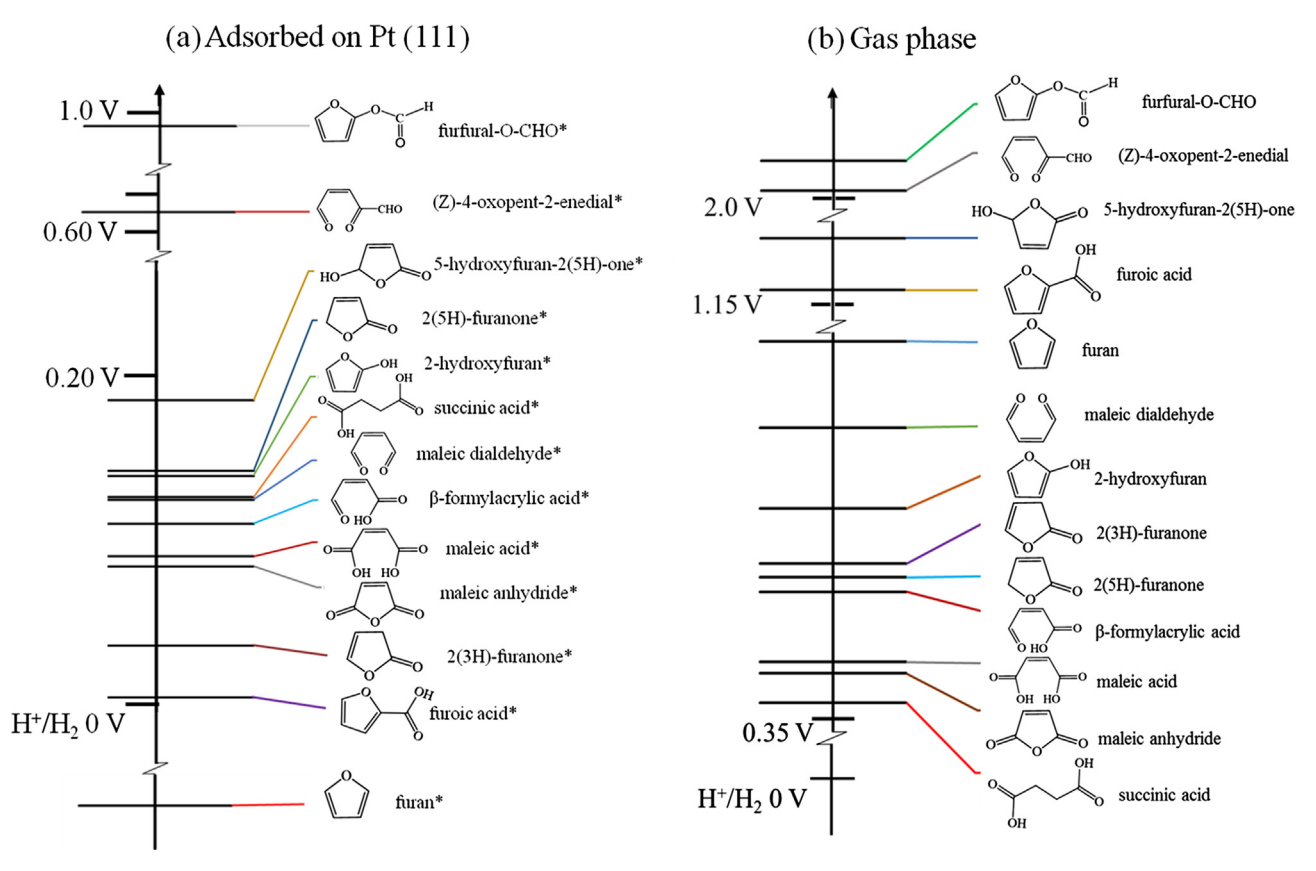


Fig. 2. The calculated equilibrium potentials for conversion of adsorbed (a) and gas phase (b) furfural* to corresponding key intermediates in furfural oxidation.

was easily formed, with an equilibrium potential close to 0 V, according to Fig. 2 and Table S3. When the applied potential is larger than 0.91 V-RHE, all the intermediates we considered (Fig. S1 and S2) are favorable to be formed on the Pt (1 1 1) surface.

Most intermediates bind to the Pt (1 1 1) surface stronger than furfural, making Pt (1 1 1) effective for motivating their formation. Their stronger binding, however, may lead to surface poisoning, as significantly higher potentials are needed to form the desorbed species for many products. Fig. 1 is also useful for determining what the most favorable intermediates, thermodynamically, are at any applied potential on the Pt (1 1 1) surface. Furan $\dot{}$ is the most stable oxidation product and favorable to be formed at any potential, whose equilibrium potential was $-0.19 \ V.$

3.4. Initial steps of furfural oxidation

Before exploring the overall reaction mechanisms, energy barriers and reaction energies of initial steps for furfural oxidation in each path at 0 V-RHE were calculated to find the most promising reaction path for furfural oxidation. The calculated activation energy barriers at different potentials are reported in Table 1. The initial reaction network, including calculated elementary reaction free energies and activation barriers at 0 V-RHE, is illustrated in Fig. 3. Structures of the initial state (IS), transition state (TS), and the finial state (FS) of each elementary step listed in Table 1 are illustrated in Fig. 4.

Path 1. Energy barriers were determined for the first three steps from furfural to adsorbed furyl intermediate. The reaction energy of the first step in Path 1from furfural (F-CHO) to F-CO at 0 V-RHE is -0.20 eV, with a barrier of only 0.55 eV. This step could happen at a reasonable rate at 0 V-RHE, and would be further accelerated at increasing oxidation potentials. In the transition state (TS2 of Path 1 in Fig. 4), the C—H distance is elongated to 1.42 Å from 1.12 Å of the initial state. The energy barrier of this dehydrogenation step on the Pt (1 1 1) surface is lower than for the same step on the Pd (1 1 1) surface (E_a = 0.95 eV) reported by Vorotnikov et al. [46], and that on the Cu (1 1 1) surface ($E_a = 0.96 \text{ eV}$) calculated by Shi et al. [47]. The activation energy barrier of this step on the Pt (111) surface is higher to that calculated on the surface of a Pt₅₅ particle ($E_a = 0.29 \text{ eV}$) [48]. The low barrier for this initial C—H dissociation step is lower than all other initial steps considered, suggesting Path 1 may be a favorable furfural oxidation path.

The second oxidation step in Path 1, forming furoic acid, is less favorable with a reaction free energy of 0.21 eV and a barrier of 0.58 eV at 0 V-RHE. The "F-CO" intermediate may also decarbonylate at this stage. But it was found that the decarbonylation barrier (E_a = 0.99 eV) on the Pt (1 1 1) surface was higher than furoic acid formation. Thus, furfural oxidation was more likely to proceed through the furoic acid formation in the Path 1 than decarbonylation of "F-CO". Our calculated energy barrier of "F-CO"

decarbonylation on Pt (1 1 1) is higher than previous values reported on Pt(1 1 1) and Cu (1 1 1) surfaces. Cai et al. reported a barrier of 0.22 eV on the Pt (1 1 1) surface for F-CO decarbonylation [48]. Their lower barrier seems to be due to beginning with a less stable adsorbed F-CO state. Vlachos and co-workers have reported a barrier of 0.68 eV on Pd (1 1 1) for this C—C scission reaction to produce adsorbed furyl intermediate species and CO [46]. Despite our higher barrier for decarbonylation, slow CO* formation (or decarbonylation motivated by higher index features) would lead to a strongly adsorbed poison that would not be oxidized from the surface until significant overpotentials.

Though decarbonylation may generate the CO* poison at low potentials, the kinetics of furoic acid formation appear favorable at any oxidative potential at which surface sites are available. The kinetic feasibility of further oxidation of furoic acid requires feasibility of decarboxylation and further steps. The decarboxylation of furoic acid removes CO₂ and a proton-electron pair. Though this appears as an oxidation step, the heterolytic (O-H) and homolytic (C—C) bond cleavages may not be concerted, separating decarboxylation into an electrochemical oxidation step and chemical step, which may occur in either order. We evaluated activation barriers for the sequential and concerted processes, and considered the inclusion of an explicit water molecule to aid heterolytic O-H dissociation. As this reaction could form three adsorbed species (furyl intermediate*, CO_2 , and H/H_3O^*), we used a 4×4 cell initially to evaluate barriers for this step, and then compared with a 3×3 cell.

We considered three routes to furoic acid decarboxylation (Fig. 6): O—H first, C—C first, and concerted. Fig. 7 shows the kinetic barriers for these paths at 0.81 V-RHE, at which reactant and product state for decarboxylation are in equilibrium. The path involving C-C cleavage first is least favorable with the highest kinetic barrier. The most feasible route for the decarboxylation involves cleaving the O-H bond first followed by C-C cleavage. The C-C cleavage barrier is 0.75 eV with 4×4 unit cell model. As this step is a chemical step, it would not be directly accelerated by an applied potential. The "concerted step" does not occur through simultaneous O—H and C—C dissociation, as the highest energy transition state (Fig. S3) had the O—H bond completely dissociated, and was equivalent to the transition state for the "O—H first" path. Moreover, addition of a single water molecule to the reaction environment accelerated the O-H cleavage while insignificantly affecting the limiting barrier (C-C cleavage), as shown in Fig. S4. We, therefore, conclude that decarboxylation of furoic acid will be slow at all potentials, limited by non-electrochemical C—C cleavage. To compare the kinetics of decarboxylation with other steps, the C—C cleavage barrier with 3×3 unit cell model was determined to be 1.11 eV. Furoic acid may be a kinetically stable product during furfural oxidation, as confirmed by initial experimental results reported in a subsequent section. Whether furoic acid will desorb

Activation energy barriers of initial steps in furfural oxidation process at potentials of 0, 0.56, 0.82, and 1.04 V-RHE. (Units: eV).

Reaction		E_a^0	U ^o	0 V	E_a		
					0.56 V	0.82 V	1.04 V
Path1	F-CHO → F-CO + H	0.39	0.32	0.55	0.27	0.14	0.03
	$F-CO + OH \rightarrow F-COOH$	0.20	0.76	0.58	0.30	0.17	0.06
	$F-CO \rightarrow \cdot F + CO$	1.00	_	1.00	1.00	1.00	1.00
	F-COOH → F-COO + H	0.78	0.31	0.93	0.65	0.52	0.41
	$F-COO \rightarrow F + CO_2$	1.11	_	1.11	1.11	1.11	1.11
Path2	F-CHO → 'F-CHO + H	1.39	0.36	1.57	1.29	1.16	1.05
	'F-CHO + OH → OH-F-CHO	0.70	0.91	1.15	0.87	0.74	0.63
Path3	$F-CHO + O \rightarrow O-F-CHO$	0.64	0.83	1.88	1.04	0.65	0.32
	O-FCHO → epoxidised-FCHO	1.00	_	1.00	1.00	1.00	1.00
Path4	F-CHO + H → F-CHOH	0.29	0.30	0.14	0.42	0.58	0.66
	F-CHOH + OH \rightarrow F-CH(OH) ₂	0.65	0.76	1.03	0.75	0.62	0.51

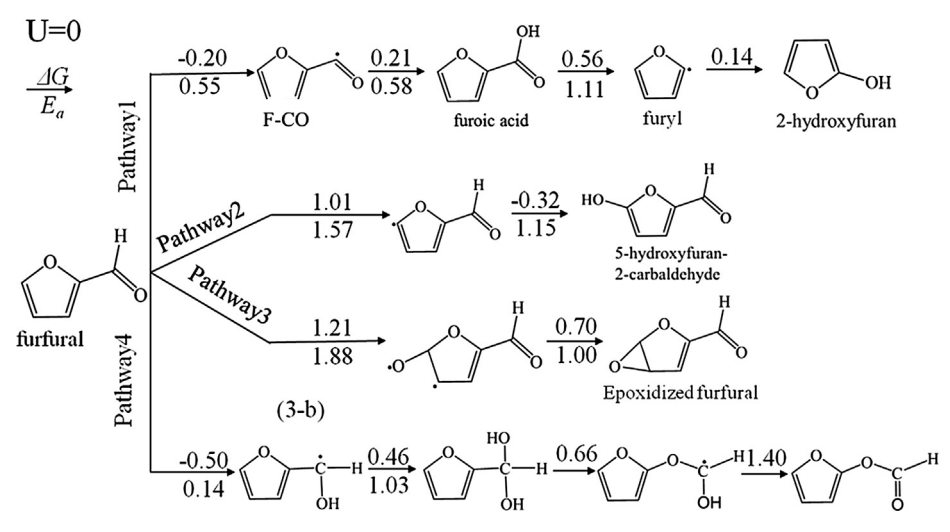


Fig. 3. Calculated elementary step reaction free energies (above arrows) and activation barriers (below arrows) of furfural oxidation in Schemes 1-4 at 0 V-RHE.

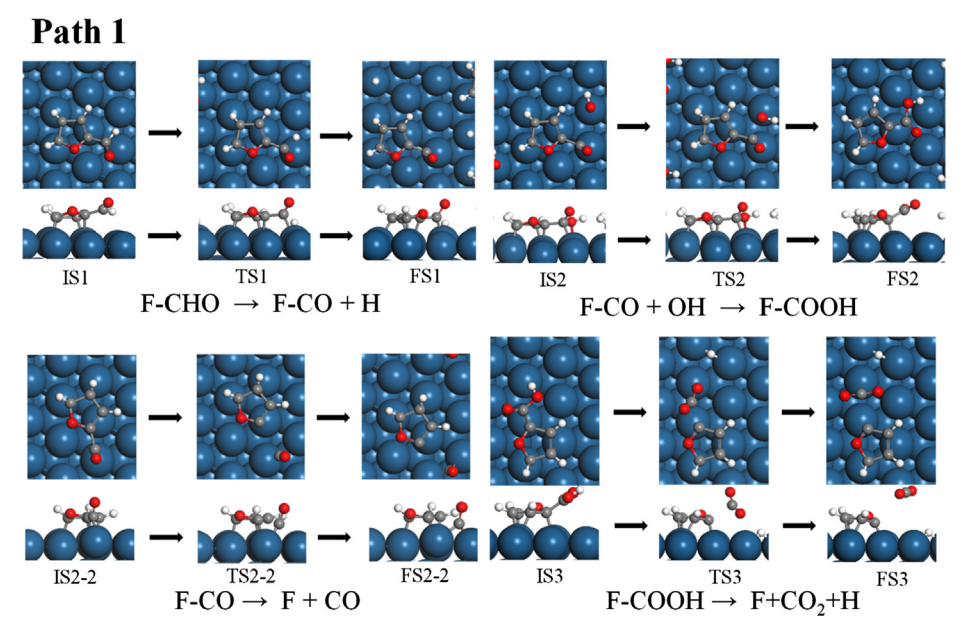


Fig. 4. Top (above) and side (below) views of all the optimized structure of the initial steps for furfural oxidation in Path 1 (Scheme 1).

as a terminal product will depend on the relative energetics to decarboxylate versus desorb. We cannot compare these energetics here, as furoic acid would desorb into an aqueous solution (if an aqueous electrolyte were used) and we do not calculate solvation free energies in this work.

Path 2. In Path 2, an H atom is initially dissociated from the furanic ring to form the furfuryl intermediate (FS1 of Path 2 in Fig. 5). The free energy of this step is 1.01 eV and the activation barrier is 1.57 eV at 0 V-RHE. Conclusively, formation of the furfuryl intermediate at 0 V-RHE is neither kinetically (1.57 vs 0.55 eV) nor thermodynamically (1.01 vs -0.20 eV) favorable compared with the first step in Path 1. If the furfuryl intermediate were formed, C—OH formation could lead to 5-hydroxyfuran-2-carbaldehyde (OH-F-CHO). This reaction is favorable due to the instability of the furfuryl intermediate ($\Delta G = -0.32$ eV at 0 V-RHE) though the barrier is still significant at 0 V-RHE due to the instability of the adsorbed OH* species at this low potential ($E_a = 1.15$ eV at 0 V-RHE).

Path 3. In the first step of Path 3, an adsorbed O atom reacts with an unsaturated double bond in the furfural ring. In the transition state (TS1 of Path 3 in Fig. 5), the O atom moves closer to a C atom of furfural and the furfural molecule is inclined from the Pt (1 1 1) surface. The calculated energy barrier at 0 V-RHE of this step is 1.88 eV, again significantly higher than that in the first step of Path 1. The reaction energy of this step, 1.21 eV at 0 V-RHE, also indicates it is not favorable. A two-electron transfer is required in this first step of Path 3 to generate the reactive O* species. Despite the two-electron nature and presumed transfer coefficient of 1.5, this step is not competitive with the initial steps of Path 1 at potentials lower than 0.56 V-RHE. The initial O* addition to the ring occurs at a single C atom, and a second step then reorganizes to form the epoxide species. The calculated reaction energy for this second step is 0.7 eV and the activation barrier for the 2nd step is 1.0 eV and can't be decreased with applied potential. We conclude that Path 3 is not competitive with Path 1 in the electrooxidation system, though Granados and co authors concluded a

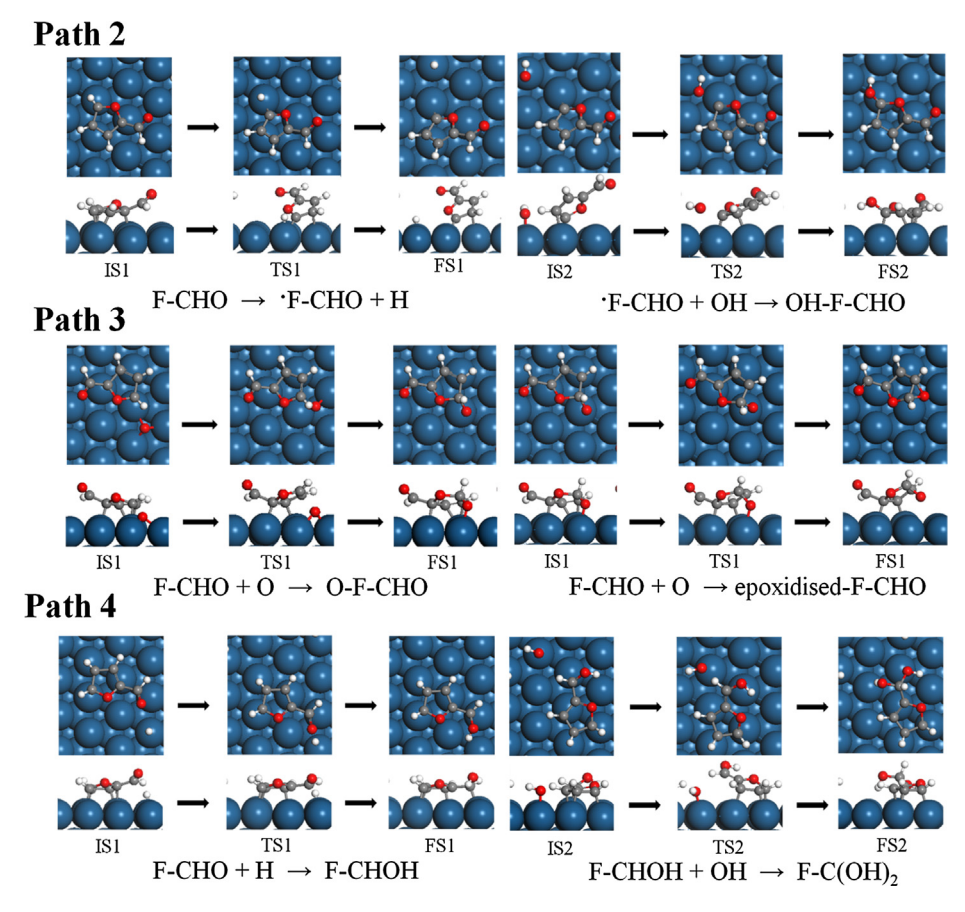


Fig. 5. Top (above) and side (below) views of all the optimized structure of the initial steps for furfural oxidation in Path 2-4 (Schemes 2-4).

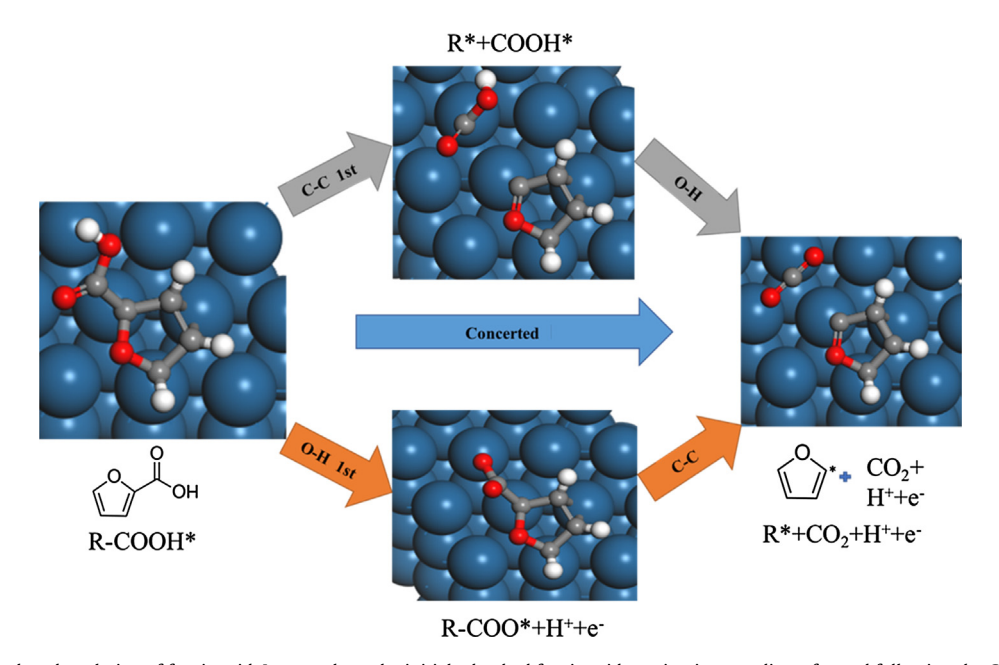


Fig. 6. Possible paths for decarboxylation of furoic acid. Images show the initial adsorbed furoic acid species, intermediates formed following the C—C or O—H dissociation routes, and the final product state for decarboxylation.

stronger oxidant, H_2O_2 , may push furfural oxidation to proceed through Path 3 [11,49].

Path 4. The first two steps in Path 4 amount to a hydrolysis reaction, with the initial step a reduction reaction adding H to the O of the carbonyl (FS1 of Path 4 in Fig. 5). The reaction energy

at 0 V-RHE for this step is $-0.50\,\text{eV}$ with a low activation barrier of 0.14 eV. The reduction of the carbonyl may be considered an equilibrated process and favorable at 0 V-RHE, however, this will become less favorable as the oxidation overpotential is increased. An additional reduction could form furfuryl alcohol with reduction

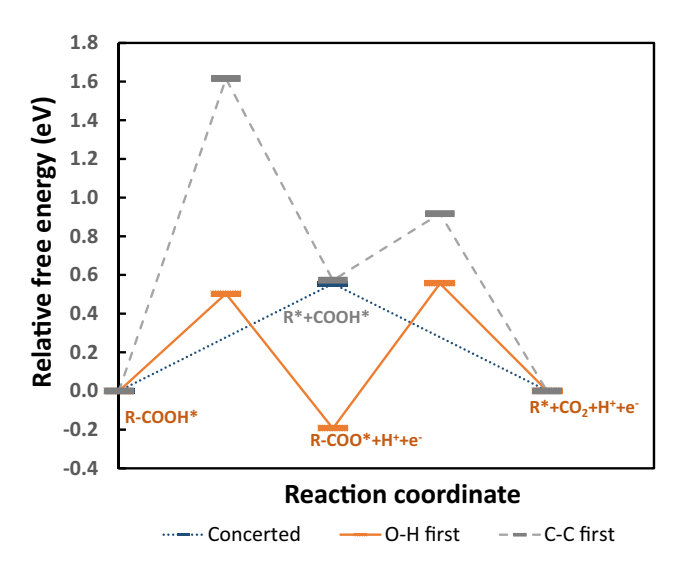


Fig. 7. Relative free energy profiles for decarboxylation of furoic acid with a 4×4 unit cell model at 0.81 V-RHE: concerted dissociation of the C—COOH and COO—H bonds (blue dotted), O—H first (orange solid) followed by C—CO₂ dissociation, and C—COOH first followed by COO—H dissociation (grey dashed). Energies in eV are relative to furoic acid and reported at 0.81 V-RHE.

favored at low potentials, though the energetics of this was not considered as our emphasis herein is oxidative processes. The barrier for the second elementary step in this path, adding an OH to the C atom of the aldehyde group of furfural, is 1.03 eV at 0 V-RHE. At 0 V-RHE, reversing the aldehyde reduction and proceeding along Path 1 will be preferred over following Path 4. The favorable initial reduction of furfural at low potentials, however, may be expected to slow oxidation. We did not investigate the barriers to further steps along Path 4, though the barrier to the next esterification step may be kinetically important. We conclude that initial barriers suggest Path 4 could be operable, though the initial reduction step will slow as oxidative potentials are applied, and kinetics of further steps would need to be considered.

Based on barriers to the initial steps, we conclude that Path 1 is the most viable path for furfural oxidation, though with still a considerable activation barrier to furoic acid decarboxylation. Initial barriers indicate Path 3 might become competitive with Path 1 at higher overpotentials, though with the favorability of the initial step of Path 1, evaluating such competition would require a more detailed kinetic analysis. High energy barriers of the initial steps in Path 2 make this path unlikely for furfural electro-oxidation on Pt(1 1 1). Even at an electrode potential of 1.0 V-RHE, the energy barriers of the rate-limiting step in Path 2 is higher than 1.0 eV, as shown in Table 1. Path 4 may be viable, but requires an initial reduction step that will slow at more oxidizing potentials, and would require future consideration of the kinetics of the esterification step that is beyond this current study. As Path 1 is the most viable based on the initial reaction energetics, the following section considers the elementary reaction energies involved in the entire Path 1. Reaction energy diagrams for furfural electro-oxidation through Paths 2, 3, 4 are given in Fig. S2-S4 in the Supporting Information.

3.5. Potential energy surface of overall reaction paths for furfural oxidation

Potential-dependent reaction free energies, including ZPVE corrections, for furfural oxidation were calculated based on Eq. (3). Reaction free energy diagrams for furfural oxidation through Path 1 at different electrode potentials are plotted in Figs. 8–11. The

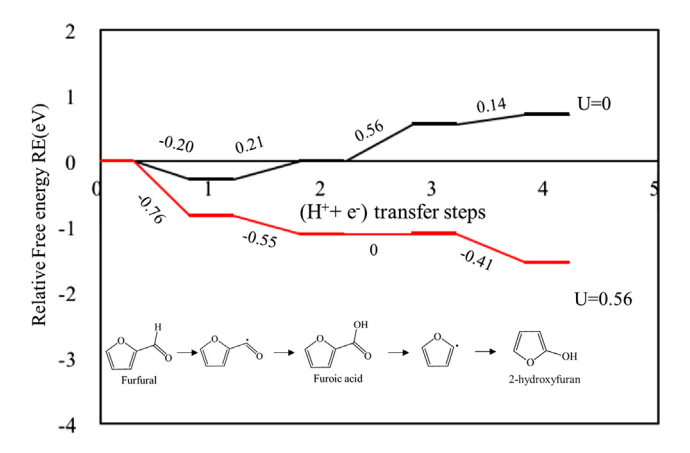


Fig. 8. The relative free energy diagrams for furfural to 2-hydroxyfuran on the Pt $(1\,1\,1)$ surface at 0 and 0.56 V-RHE.

reaction energy diagram for furfural conversion to 2-hydroxyfuran in Path 1 is given in Fig. 8. Reaction diagrams for 2-hydroxyfuran conversion to maleic acid, maleic anhydride, and succinic acid through Paths 1-A, 1-B, and 1-C are plotted in Figs. 9–11, respectively. Barriers were not considered in this analysis, though we find reaction free energies are sufficient to make initial conclusions on the most possible reaction paths and products for furfural oxidation in the electrocatalytic system.

Path 1-A. Reaction free energy diagrams at 0 V and 0.56 V-RHE for furfural electro-oxidation through Path 1-A are shown in Figs. 8 and 9. At 0 V-RHE, the majority of steps are uphill. The most thermodynamically unfavorable electrochemical step is decarboxylation of furoic acid, with a reaction energy of 0.56 eV at 0 V-RHE. All electrochemical steps from furfural to 2-hydroxyfuran in Path 1-A are exergonic when the applied electrode potential is 0.56 V or higher. The non-electrochemical furoic acid decarboxylation step, as discussed in the previous section, will have a high C—C dissociation barrier of 1.11 eV. The non-electrochemical reaction energy for conversion of 2-hydroxyfuran to epoxidized furan ($\Delta G = 1.12 \text{ eV}$) is also unfavorable and would not be affected by an increased oxidation potential. These unfavorable nonelectrochemical energetics are consistent with the slow oxidation of furoic acid to epoxidized furan observed experimentally by Granados and co-authors [11]. Path 1 may be expected to rapidly produce furoic acid at oxidation overpotentials, but oxidation through Path 1-A might not be favorable to continue to maleic acid even at higher potentials.

Path 1-B. The reaction free energy diagram for further conversion of 2-hydroxyfuran to succinic acid through Path 1-B is given in Fig. 10. In Path 1-B, 2-hydroxyfuran is converted to 2(3H)furanone rather than to epoxidized furan, and the eventual oxidation of 2(3H)-furanone produces succinic acid. Through Path 1-B, the most thermodynamically unfavorable electrochemical step at 0 V-RHE is the step of 2(3H)-furanone oxidation accompanied by furan ring opening (0.82 eV at 0 V-RHE). All electrochemical steps in Path1-B would be downhill when the applied potential is 0.82 V-RHE or higher. Furyl intermediate formation at 0.82 V-RHE would be thermodynamically favorable. The reaction free energy of 2-hydroxyfuran conversion to 2(3H)-furanone as the fourth step of Path 1-B is negative, as illustrated in Fig. 3 $(\Delta G = -0.53 \text{ eV})$, which implies that the formation of 2(3H)furanone is thermodynamically favorable. Furyl intermediate formation and ring-opening of 2(3H)-furanone is favorable at 0.82 V-RHE. However, the formation of trans-4-hydroxycrotonic acid includes a reduction step that becomes less favorable with increasing potentials, including a positive reaction free energy of

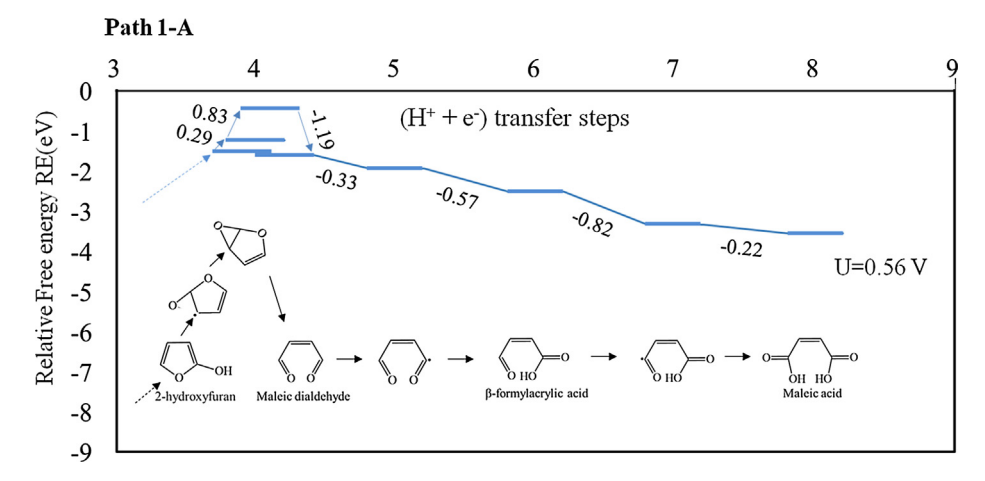


Fig. 9. Reaction diagrams for 2-hydroxyfuran conversion to maleic acid in Path 1-A on the Pt (1 1 1) surface at 0.56 V-RHE.

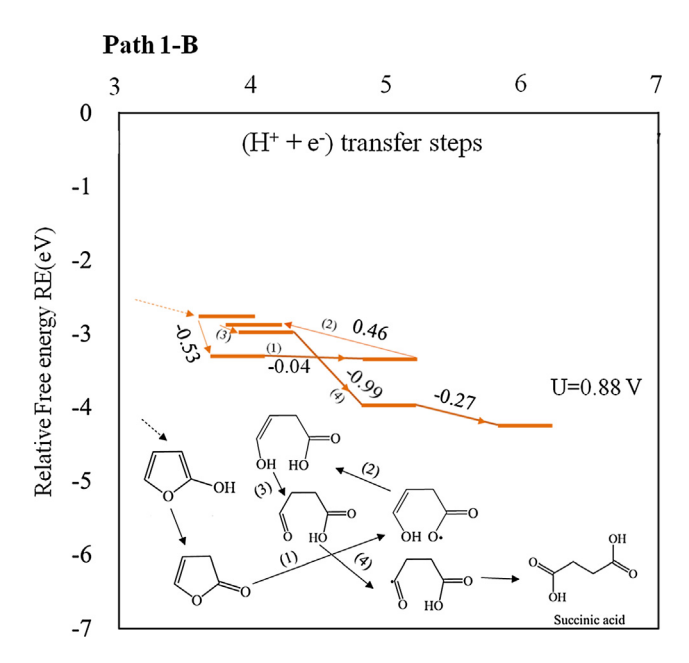


Fig. 10. Reaction diagrams for 2-hydroxyfuran conversion to succinic acid in Path 1-B on the Pt $(1\ 1\ 1)$ surface at $0.88\ V$ -RHE.

0.48 eV at 0.88 V-RHE. This value is not necessarily unsurmountable at 0.82 V-RHE, and the subsequent favorable steps could drive furfural oxidation to succinic acid. Therefore, there is likely an intermediate overpotential range at which furfural oxidation to succinic acid through Path 1-B is thermodynamically viable. However, when increasing the applied electrode potential, the reduction step required to form trans-4-hydroxycrotonic acid formation will become less favorable, and will arrest this process at 2-hydroxyfuran or a furan-one isomer. The need to balance elementary oxidation and reduction rates to control eventual product formation suggests the possibility of using electrode potential to control oxidation selectivity (presuming all species remain on the surface rather than involving solution phase hydration/hydrolysis reactions).

Path 1-C. The reaction energy diagrams for furfural oxidation to maleic acid and maleic anhydride through Path 1-C are given in Fig. 11. In Path 1-C, 2-hydroxyfuran isomerizes to 2(5H)-furanone which finally oxidizes to maleic acid. The reaction free energy of 2-hydroxyfuran conversion to 2(5H)-furanone is 0.02 eV, indicating that 2(5H)-furanone formation is thermodynamically possible, though less favorable than 2(3H)-furanone formation (-0.53 eV).

The most thermodynamically unfavorable step at 0 V-RHE for Path 1-C is the formation of hydroxy-furanone from furan-2(5H)-one, with a reaction energy of 1.04 eV. All steps in Path 1-C are energetically downhill at an applied electrode potential of 1.04 V-RHE, which indicates that all elementary steps for furfural oxidation to maleic acid and maleic anhydride are thermodynamically feasible at applied potentials of 1.04 V-RHE and above. All steps in Path 1-C are either oxidations or favorable isomerizations, such that increasing overpotential will act only to accelerate this oxidation reaction.

Comparing Paths 1- A, B, C, overall oxidation kinetics might be limited by furoic acid decarboxylation at these oxidation overpotentials (0.56, 0.82, 1.04 V-RHE). Initial aldehyde C-H activation (Path 1) or carbonyl oxygen reduction (Path 4) are thermodynamically favorable at these overpotentials, possibly resulting in formation of intermediates on the surface that could undergo unselective oligomerization reactions. The non-electrochemical decarbonylation of furfural to furan may also be operable at low overpotentials, with the rates of the individual oxidation and reduction steps involved in this path still influenced by the electrode potential. Overpotentials near 0.82 V and 1.02 R-RHE could allow for ring-opening reactions of 2(3H)-furanone in Path 1-B and 5-OH-furan-2(5H)-one formation in Path 1-C. Subsequent reactions through Path 1-B and Path 1-C could produce succinic acid and maleic acid. Favorable 2-hydroxylfuran isomerization to 2(3H)-furanone could drive succinic acid formation at intermediate overpotentials. However, further increase in overpotential could slow succinic acid formation in Path 1-B due to the involvement of a reduction step (presuming no solution phase transformation), making the relative rate of maleic acid formation via 2(5H)furanone in Path 1-C dominant. Selectivity to succinic acid (lower overpotentials) or maleic acid (higher overpotentials) may be tunable in the electro-oxidation system similar to tuning the H₂O₂/furfural ratio or other reaction conditions in non-electrochemical oxidation experiments [11,38,39].

Paths 2–4. Reaction free energy diagrams for Path 2–4 are given in Figs. S5–S7. As discussed above, these processes are limited by high barriers to initial elementary steps. If applied overpotentials are sufficient to drive these initial steps, the remaining elementary steps are favorable, suggesting multiple paths to maleic acid and maleic anhydride may be operable at high overpotentials.

3.6. Experimental results

Faradaic efficiency obtained at 0.9 V-RHE on nanoparticle Pt/C during electrochemical oxidation of furfural is reported in Fig. 12.

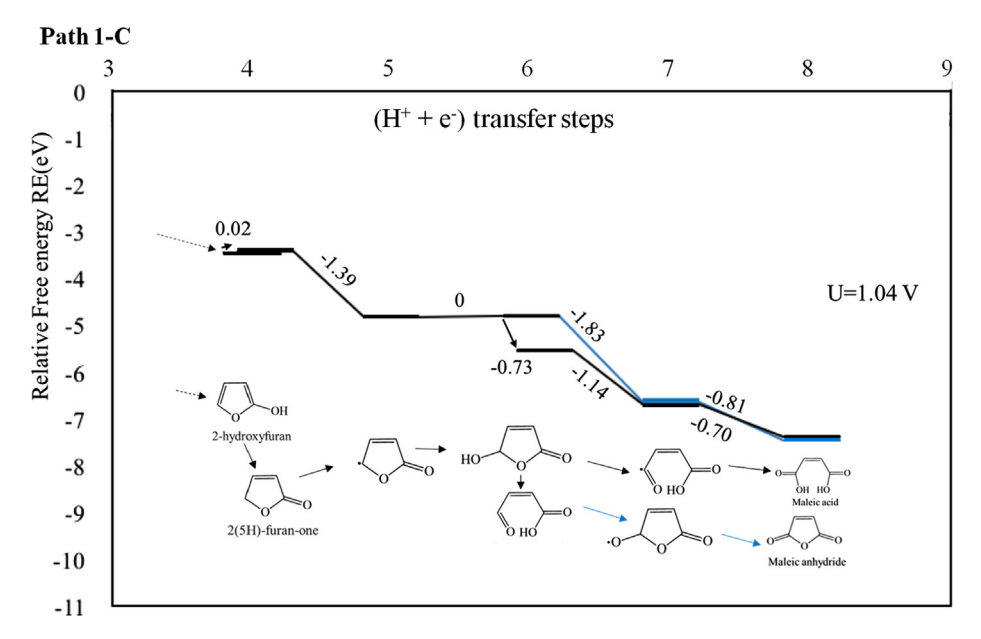


Fig. 11. Reaction diagrams for 2-hydroxyfuran conversion to maleic acid and maleic anhydride in Path 1-C on the Pt (1 1 1) surface at 1.04 V-RHE.

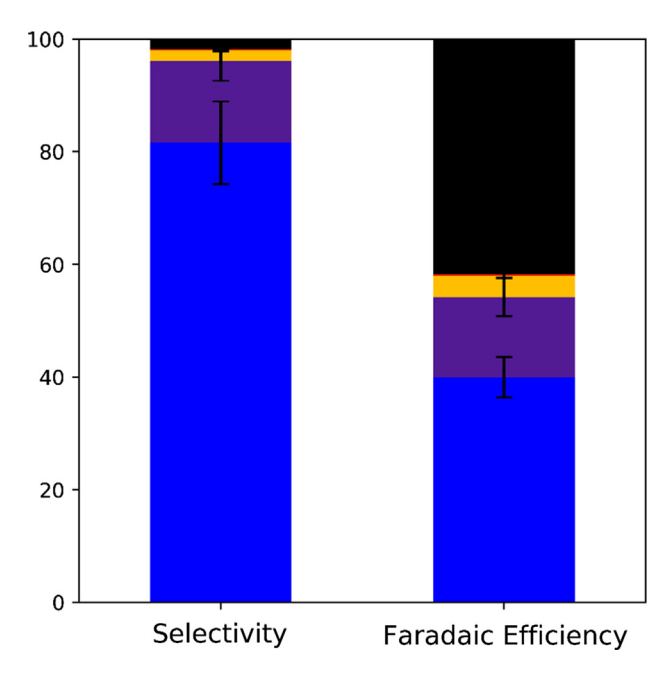


Fig. 12. Selectivity (per consumed furfural molecule) and Faradaic efficiency during electrocatalytic oxidation of furfural over Pt/C at 0.9 V-RHE. Blue (Furoic Acid), Purple (5-Hydroxyfuroic Acid), Yellow (Maleic Acid), Orange (5-Hydroxy-furan-2 (5H)-one), and Black (Unaccounted electron balance/CO₂).

At potentials less than 0.9 V-RHE, a negligible oxidation current was observed. This observation is qualitatively consistent with surface poisoning due to adsorbed CO formed by decarbonylation of furfural at lower potentials. Above 0.9 V-RHE, a significant amount of current is directed to furoic acid production, with relatively smaller amount to further oxidized products such as maleic acid, 5-hydroxyfuroic acid, and 5-hydroxyfuran-2(5H)-one detected. The high selectivity to furoic acid is consistent with DFT energetics suggesting its formation is facile and there is a high non-electrochemical kinetic barrier to decarboxylation. 5-hydroxyfuroic acid would be produced by ring oxidation, and its presence further suggests furoic acid decarboxylation could be a

limiting step. Our DFT analysis did not consider paths to 5-hydroxyfuroic acid as we found ring oxidation slow in Path 2. However, these paths may be accelerated by the presence of surface O at higher potentials, which we leave for future DFT studies.

The other experimentally observed products are also consistent with DFT energetics. Both 5-hydroxyfuran-2(5H)-one and maleic acid can be formed through Path 1-C, which showed viable DFT reaction energies at 0.9 V-RHE. Further studies of potential and electrolyte dependent product distributions, and additional DFT consideration of oxygen covered Pt surfaces will help to clarify furfural oxidation paths at high overpotentials.

4. Conclusions

Periodic DFT calculations were performed for the adsorption energies, relative free energies of key intermediates and reaction energies of furfural oxidation in an electrocatalytic system on the Pt (1 1 1) surface. Comparing four paths of furfural oxidation, formation of furoic acid is expected due to favorable energetics for its formation and significant barriers to subsequent decarboxylation steps. Furfural oxidation past the furoic acid intermediate is calculated to proceed through Path 1-B to succinic acid via 2 (3H)-furanone as an intermediate and Path 1-C to maleic acid and maleic anhydride via 2(5H)-furanone as an intermediate. Intermediate overpotentials (around 0.82 V-RHE) may drive succinic acid formation through Path 1-B, with Path 1-C to maleic acid dominant at higher overpotentials. Our results based on the kinetics of the initial steps provide a good indication to the dominant mechanism responsible for furfural oxidation initiation, which is consistent with the initial product distribution observed experimentally. In addition, the thermodynamics of all surface adsorbed intermediates allows us a reasonable estimate for favorability of different products in the range of applied potentials. Though this initial study provides some indication of plausible electrooxidation paths for furfural oxidation on the Pt (111) surface, a number of limitations should be highlighted. The lack of the inclusion of solvation of surface bound intermediates could alter the relative energies of various species by significant amounts, which are challenging to estimate. Difficulties in representing the ensemble of water structures present at the metal-electrolyte interface,

together with the unreliability of parametrized continuum solvation models, makes estimating the associated error challenging. Specific effects of ions in the interfacial region as well as interfacial electric fields are also neglected, and our approach to electrochemical activation barriers is inherently approximate and was only applied to initial reaction steps due to the computational intensity of considering so many possible reaction steps. Conclusions of dominant reaction paths are also limited without detailed microkinetic modeling. Significant coverage of water oxidation products (O*, OH*, or surface oxides) may be present at oxidizing potentials above 0.6 V-RHE on Pt electrodes. Despite these limitations, the results presented provide an initial indication of likely electrooxidation paths of such complex molecules, and motivate future work to improve on these limitations, while this work guides the selection of reaction paths subjected to further scrutiny.

Acknowledgements

L. Gong acknowledges scholarship from the China Scholarship Council for a joint PhD student. Financial support from the National Science Foundation, Grant # 1665155 is acknowledged. This work used the Extreme Science and Engineering Discovery Environment (XSEDE), supported by National Science Foundation grant number ACI - 1053575. N. A. acknowledges training provided by the Computational Materials Education and Training (CoMET) NSF Research Traineeship (Grant No. DGE-1449785).

Appendix A. Supplementary material

Supplementary data to this article can be found online at https://doi.org/10.1016/j.jcat.2019.04.012.

References

- [1] S.R. Collinson, W. Thielemans, The catalytic oxidation of biomass to new materials focusing on starch, cellulose and lignin, Coordin, Chem. Rev. 254 (2010) 1854-1870.
- [2] M.J. Climent, A. Corma, S. Iborra, Converting carbohydrates to bulk chemicals and fine chemicals over heterogeneous catalysts, Green Chem. 13 (2011) 520-540.
- [3] R. Mariscal, P. Maireles-Torres, M. Ojeda, I. Sádaba, M. López Granados, Furfural: a renewable and versatile platform molecule for the synthesis of chemicals and fuels, Energy Environ. Sci. 9 (2016) 1144-1189.
- [4] X.D. Li, P. Jia, T.F. Wang, Furfural: a promising platform compound for sustainable production of C-4 and C-5 chemicals, ACS Catal. 6 (2016) 7621-7640
- [5] I. Bechthold, K. Bretz, S. Kabasci, R. Kopitzky, A. Springer, Succinic acid: a new platform chemical for biobased polymers from renewable resources, Chem. Eng. Technol. 31 (2008) 647-654.
- [6] G. Centi, F. Trifiro, J.R. Ebner, V.M. Franchetti, Mechanistic aspects of maleicanhydride synthesis from C4-hydrocarbons over phosphorus vanadium-oxide, Chem. Rev. 88 (1988) 55-80.
- [7] S. Shi, H.J. Guo, G.C. Yin, Synthesis of maleic acid from renewable resources: catalytic oxidation of furfural in liquid media with dioxygen, Catal. Commun. 12 (2011) 731-733.
- [8] N. Alonso-Fagundez, M.L. Granados, R. Mariscal, M. Ojeda, Selective conversion of furfural to maleic anhydride and furan with VOx/Al2O3 catalysts, Chemsuschem 5 (2012) 1984-1990.
- [9] X.K. Li, B. Ho, Y.G. Zhang, Selective aerobic oxidation of furfural to maleic anhydride with heterogeneous Mo-V-O catalysts, Green Chem. 18 (2016) 2976-2980.
- [10] H. Guo, G. Yin, Catalytic aerobic oxidation of renewable furfural with phosphomolybdic acid catalyst: an alternative route to maleic acid, J. Phys. Chemi, C 115 (2011) 17516-17522.
- [11] N. Alonso-Fagúndez, I. Agirrezabal-Telleria, P.L. Arias, J.L.G. Fierro, R. Mariscal, M.L. Granados, Aqueous-phase catalytic oxidation of furfural with H2O2: high yield of maleic acid by using titanium silicalite-1, RSC Adv. 4 (2014) 54960-54972.
- [12] J. Lan, Z. Chen, J. Lin, G. Yin, Catalytic aerobic oxidation of renewable furfural to maleic anhydride and furanone derivatives with their mechanistic studies, Green Chem. 16 (2014) 4351-4358.
- [13] H.G. Cha, K.S. Choi, Combined biomass valorization and hydrogen production in a photoelectrochemical cell, Nat. Chem. 7 (2015) 328-333.

- [14] N. Jiang, B. You, R. Boonstra, I.M.T. Rodriguez, Y.J. Sun, Integrating electrocatalytic 5-hydroxymethylfurfural oxidation and hydrogen production via Co-P-derived electrocatalysts, ACS Energy Lett. 1 (2016) 386-390.
- [15] A.C. Garcia, M.J. Kolb, C.V.Y. Sanchez, J. Vos, Y.Y. Birdja, Y. Kwon, G. Tremiliosi-Filho, M.T.M. Koper, Strong impact of platinum surface structure on primary and secondary alcohol oxidation during electro-oxidation of glycerol, ACS Catal. 6 (2016) 4491-4500.
- [16] S. Lee, H.J. Kim, E.J. Lim, Y. Kim, Y. Noh, G.W. Huber, W.B. Kim, Highly selective transformation of glycerol to dihydroxyacetone without using oxidants by a PtSb/C-catalyzed electrooxidation process, Green Chem. 18 (2016) 2877-2887.
- [17] Y. Kwon, K.J.P. Schouten, J.C. van der Waal, E. de Jong, M.T.M. Koper, Electrocatalytic conversion of furanic compounds, ACS Catal. 6 (2016) 6704-
- [18] A.C. Chen, P. Holt-Hindle, Platinum-based nanostructured materials: synthesis, properties, and applications, Chem. Rev. 110 (2010) 3767-3804.
- [19] H. Li, F. Calle-Vallejo, M.J. Kolb, Y. Kwon, Y. Li, M.T.M. Koper, Why (1 0 0) terraces break and make bonds: oxidation of dimethyl ether on platinum single-crystal electrodes, J. Am. Chem. Soc. 135 (2013) 14329-14338
- [20] J.A. Herron, P. Ferrin, M. Mavrikakis, First-principles mechanistic analysis of dimethyl ether electro-oxidation on monometallic single-crystal surfaces, J. Phys. Chem. C 118 (2014) 24199-24211.
- Strasser, Oxidation of biomass derived 5-Vuyyuru, hydroxymethylfurfural using heterogeneous and electrochemical catalysis, Catal. Today 195 (2012) 144-154.
- [22] A.H. Blaesi, C.R. Buie, Characterization of the electrochemical oxidation of glucose on Pt nanoparticle catalysts in pH neutral phosphate buffer solution, ECS Trans. 33 (2011) 41-48.
- [23] P.E. Blochl, Projector augmented-wave method, Phys. Rev. B 50 (1994) 17953-
- [24] G. Kresse, D. Joubert, From ultrasoft pseudopotentials to the projector augmented-wave method, Phys. Rev. B 59 (1999) 1758-1775.
- [25] J.P. Perdew, J.A. Chevary, S.H. Vosko, K.A. Jackson, M.R. Pederson, D.J. Singh, C. Fiolhais, Atoms, molecules, solids, and surfaces-applications of the generalized gradient approximation for exchange and correlation, Phys. Rev. B 46 (1992) 6671-6687.
- [26] A. Gulans, M.J. Puska, R.M. Nieminen, Linear-scaling self-consistent implementation of the van der Waals density functional, Phys. Rev. B 79
- [27] G. Kresse, J. Furthmuller, Efficient iterative schemes for ab initio total-energy calculations using a plane-wave basis set, Phys. Rev. B 54 (1996) 11169-
- [28] G. Kresse, J. Furthmuller, Efficiency of ab-initio total energy calculations for metals and semiconductors using a plane-wave basis set, Comp. Mater. Sci. 6 (1996) 15-50.
- [29] G. Kumar, C.H. Lien, M.J. Janik, J.W. Medlin, Catalyst site selection via control over noncovalent interactions in self-assembled monolayers, ACS Catal. 6 (2016) 5086-5094.
- [30] G. Henkelman, B.P. Uberuaga, H. Jonsson, A climbing image nudged elastic band method for finding saddle points and minimum energy paths, J. Chem. Phys. 113 (2000) 9901-9904.
- [31] J.K. Norskov, J. Rossmeisl, A. Logadottir, L. Lindqvist, J.R. Kitchin, T. Bligaard, H. Jonsson, Origin of the overpotential for oxygen reduction at a fuel-cell cathode, J. Phys. Chem. B 108 (2004) 17886–17892.
- [32] D. McQuarrie, Statistical Mechanics University Science Books, Sausalito, CA. (2000) pp. 222-223.
- [33] G. Rostamikia, A.J. Mendoza, M.A. Hickner, M.J. Janik, First-principles based microkinetic modeling of borohydride oxidation on a Au(111) electrode, J. Power Sources 196 (2011) 9228-9237.
- [34] I. Merino-Jimenez, M.J. Janik, C.P. de Leon, F.C. Walsh, Pd-Ir alloy as an anode
- material for borohydride oxidation, J. Power Sources 269 (2014) 498–508. [35] X.W. Nie, W.J. Luo, M.J. Janik, A. Asthagiri, Reaction mechanisms of CO2 electrochemical reduction on Cu(111) determined with density functional theory, J. Catal. 312 (2014) 108-122.
- [36] H.J. Guo, G.C. Yin, Catalytic Aerobic Oxidation of Renewable furfural with phosphomolybdic acid catalyst: an alternative route to maleic acid, J. Phys. Chem. C 115 (2011) 17516-17522.
- [37] J.H. Lan, Z.Q. Chen, J.C. Lin, G.C. Yin, Catalytic aerobic oxidation of renewable furfural to maleic anhydride and furanone derivatives with their mechanistic studies, Green Chem. 16 (2014) 4351-4358.
- [38] H. Choudhary, S. Nishimura, K. Ebitani, Highly Efficient Aqueous oxidation of furfural to succinic acid using reusable heterogeneous acid catalyst with hydrogen peroxide, Chem. Lett. 41 (2012) 409-411.
- [39] H. Choudhary, S. Nishimura, K. Ebitani, Metal-free oxidative synthesis of succinic acid from biomass-derived furan compounds using a solid acid catalyst with hydrogen peroxide, Appl. Catal. A-Gen. 458 (2013) 55-62.
- [40] J.J. Baschuk, X.G. Li, Carbon monoxide poisoning of proton exchange membrane fuel cells, Int. J. Energ. Res. 25 (2001) 695–713.
- [41] M.J. Taylor, L.J. Durndell, M.A. Isaacs, C.M.A. Parlett, K. Wilson, A.F. Lee, G. Kyriakou, Highly selective hydrogenation of furfural over supported Pt nanoparticles under mild conditions, Appl. Catal. B-Environ. 180 (2016) 580-585.
- [42] B. Liu, L. Cheng, L. Curtiss, J. Greeley, Effects of van der Waals density functional corrections on trends in furfural adsorption and hydrogenation on close-packed transition metal surfaces, Surf. Sci. 622 (2014) 51-59.
- [43] C.M. Horiuchi, M. Rangan, B.M. Israel, J.W. Medlin, Adsorption and decomposition of 2(5H)-furanone on Pd(111) and Pt(111): comparison of

- ring-opening pathways of an unsaturated cyclic ester, J. Phys. Chem. C 113 (2009) 14900–14907.
- [44] G. Sinha, O. Heikkinen, M. Vestberg, L. Mether, K. Nordlund, J. Lahtinen, Adsorption of maleic anhydride on Pt(111), Surf. Sci. 620 (2014) 9–16.
- [45] V. Pallassana, M. Neurock, First-principles periodic density functional study of the hydrogenation of maleic anhydride to succinic anhydride over palladium (111), J. Phys. Chem. B 104 (2000) 9449–9459.
- [46] V. Vorotnikov, G. Mpourmpakis, D.G. Vlachos, DFT study of furfural conversion to furan, furfuryl alcohol, and 2-methylfuran on Pd(111), Acs Catal. 2 (2012) 2496-2504.
- [47] Y. Shi, Y. Zhu, Y. Yang, Y.-W. Li, H. Jiao, Exploring furfural catalytic conversion on Cu(111) from computation, ACS Catal. 5 (2015) 4020–4032.
 [48] Q.X. Cai, J.G. Wang, Y.G. Wang, D.H. Mei, Mechanistic insights into the structure-dependent selectivity of catalytic furfural conversion on platinum catalysts, AIChE. J. 61 (2015) 3812-3824.
- [49] N. Alonso-Fagundez, I. Agirrezabal-Telleria, P.L. Arias, J.L.G. Fierro, R. Mariscal, M.L. Granados, Aqueous-phase catalytic oxidation of furfural with H2O2: high yield of maleic acid by using titanium silicalite-1, RSC Adv. 4 (2014) 54960-54972.